CHAPTER IV

MEASUREMENT OF FLEXOELECTRIC COEFFICIENTS OF SOME NEMATIC LIQUID CRYSTALS

4.1 Introduction

As we have discussed in Chapter I of this thesis, the nematic director is apolar. Hence the usual dielectric coupling with an external electric field depends quadratically on the latter. However, as has been discussed earlier a deformed director field with a splay and/or bend distortion can lead to a flexoelectric polarisation of the medium. The response of liquid crystals to an electric field under many circumstances is influenced by the flexoelectric effect. In this case the coupling is linear with the applied electric field as well as the curvature of the director field. In fact this special feature produces many interesting effects on electrohydrodynamic (EHD) instabilities (Madhusudana et al., 1987,1989; Raghunathan *et* al., 1991), which has been discussed in the previous chapters.

It is therefore obviously of considerable interest to measure flexoelectric coefficients of nematic liquid crystals (NLC). Though there have been a few earlier measurements of these coefficients there has not been any systematic measurements

on any homologous series. There are several theoretical models (Straley, 1976; Osipov, 1983, 1984; Singh et al., 1989; Nemtsov et al., 1986; Helfrich, 1971a, 1971b, 1974), which relate flexoelectric coefficients with the orientational order parameter (S) and molecular properties. We summarise these theoretical models below and in the subsequent section we describe experimental techniques of measurement of flexoelectric coefficients. We have also made an attempt to compare our results which are reported in the last section with the theoretical predictions.

As we have described in Chapter I, splay and bend distortions of the director field in a nematic liquid crystal can induce a flexoelectric polarisation given by (Meyer, 1969),

$$\vec{P} = e_1\hat{n}(\nabla \cdot \hat{n}) + e_3(\nabla \times \hat{n}) \times \hat{n} \qquad (4.1)$$

where e_1 and e_3 are the flexoelectric coefficients corresponding to splay arid bend distortions respectively. This flexoelectric polarisation $\vec{P}$, cannot be measured directly by using a distorted nematic because of the screening of the polarisation charges by small traces of impurity ions present in the sample. Therefore, usually the inverse effect, viz., the flexoelectric distortion of the director configuration induced by an external electric field, is used to measure the flexoelectric coefficients.

As discussed in Chapter I, both the electric dipole moments and quadrupolar moments of the molecules contribute to flexoelectric effect. According to some of the models, to a good approximation, the quadrupolar contribution gives rise to the combination $(e_1 + e_3)$ of the flexoelectric coefficients and hence the difference combination $(e_1 - e_3)$ of the coefficients is mainly determined by the dipolar contribution (e_d^*). Osipov (1983) showed that the main contribution to e_d^* conies from the transverse dipole moment $(\mu_\perp)$ of banana shaped molecules rather than from their longitudinal dipole moments (Fig.4.1, see after page 70). Indeed, he has argued

that e_d^* should be very small for compounds with zero transverse dipole moment. Further, he has also shown that e_d^* is proportional to the molecular length. More recently similar conclusions were drawn by Singh and Singh (1989) using a density functional formalism to calculate flexoelectric coefficients.

The relationship between the flexoelectric effect and orientational order parameter (S) is discussed in several theoretical papers. Earlier phenomenological models of the dipolar contribution e(; in molecules with rigid structures indicated an S^2 dependence (Straley, 1976; Osipov 1983, 1984). On the other hand, the leading contribution from the quadrupolar density of the nematic medium varies as S (Prost *et* al., 1977). Osipov (1983) made detailed molecular calculations by including both short range repulsive and attractive interactions between molecules with shape asymmetrics and concluded that in general the flexoelectric coefficients liave terms depending on both S and S^2. (Even the purely quadrupolar effect can give rise to an S^2 dependence due to the tensor nature of the Lorentz factor in tlie anisotropic medium.)

Marcerou and Prost (1980) have devised an interdigitated electrode technique to measure the intensity of light scattering produced by the spatially periodic flexoelcctric distortion due to an applied AC field. They could calculate $(e_1 + e_3)$ from their experiment. Further they also demonstrated that a symmetric tolane compound which does not have a net dipole moment has a fairly large value of (el $+ e_3$), arising from the quadrupole moment. More interestingly even in cases with permanent dipoles and hence a non-zero value of the dipolar contribution, $(e_1 + e_3)$ was found to be nearly proportional to S, thus demonstrating that this combination of tlie flexoelectric coefficients arises mainly from tlie quadrupolar effect. But the sign of $(e_1 + e_3)$ is not determined by this technique. Later Dozov *et al.* (1984)

used a simple electrode configuration to generate a field gradient and determined the sign of $(e_1 + e_3)$ of MBBA to be negative. This sign has been confirmed by the later measurement of $(e_1 + e_3)$ by an optical technique on a hybrid aligned cell with weak anchoring (Madhusudana and Durand, 1985; Barbero et *al.*, 1986). Beresriev et al. (1987), using a pyroelectric technique, have measured $(e_1 + e_3)$ of MBBA, though there is no mention of its sign. Recently e_1 and e_3 measuremerits have also been made by a technique based on an acoustic wave induced periodic deformation (Skaldin et al., 1985, 1990). The values of e_1 and e_3 determined by this technique are relatively high; but their signs have not been determined.

Dozov et al. (1982, 1983) devised a simple experimental technique of measuring $e^* = (e_1 - e_3)$, which arises mainly from the dipolar contributions to flexoelectricity. Following are some of the interesting results of their study.

1. Octylcyanobiphenyl (8CB), which has a strong terminal dipole moment (-C ≡ N) has a value of e* comparable to that of MBBA, which has a significant lateral dipole.

2. Both 8CB and MBBA have a temperature independent value of (e^*/K), wliere K is an elastic constant and hence $e^* \propto \mathbf{S}^2$ as expected of the dipolar contribution (Dozov et al., 1983).

3. e^*/K has a negative sign for octyloxy cyanobiphenyl (8OCB), which has an octyloxy chain giving rise to a transverse component of the dipole moment. Further e^*/K increases with temperature indicating that $e^* \propto S$. Though $(e_1 + e_3)$ of 8OCB is proportional to S, the latter result arises from the fact that the main contribution to $(e_1 + e_3)$ come from quadrupolar effects. c* on the other hand has a significant contribution from the dipolar effect and the observed S-dependence was attributed to the flexibility of the octyloxy chain.

Osipov (1984) has confirmed that the inclusion of the flexibility of molecules can give rise to an additional S^{-1} dependence of c*. If this is the dominating factor, e*

becomes proportional to S. Nemtsov and Osipov (1986) have developed a general correlation function approach to calculate e_1 and e3. In particular, they argue that the additional transverse dipole moment of 8OCB can give rise to the reversal of the sign of e* compared to that of 8CB.

4.2 Experimental Techniques

4.2.1 Measurement of $(e_1 - e_3)$

We have used the method of Dozov et *al.* (1982) for the measurement of e^*/K_2, where e* = $(e_1 - e_3)$ and K_2 is the twist elastic constant. The geometry of the sample is as shown in figure 4.2. The plate A is coated with polyimide and unidirectionally rubbed to get homogeneous alignment and the Plate B is coated with ODSE (octadecyl triethoxy silane) to get homeotropic alignment. The anchoring is assumed to be strong at the two surfaces. In such a hybrid aligned nematic (IIAN) cell, the director field has a permanent splay-bend distortion, which gives rise to a flexoelectric polarisation $\vec{P}$ along the X-axis given by,

$$\vec{P} = (e_1 - e_3)\hat{n}\, div\, \hat{n} \ . \qquad (4.2)$$

If a vertical field (along the Z axis) is applied between plates of a HAN cell, the flexoelectric energy (-P.E), which is linear in curvature $\frac{d\theta}{dz}$ depends only on one distortion angle θ and its derivative, and the corresponding contribution to bulk torque density is zero. On the other hand, when an electric field is applied along the Y-direction, a twist (ϕ) distortion is produced in the medium due to the action of $\vec{E}$ on $\vec{P}$ (Fig.4.3) and in such a case, the flexoelectric effect contributes to the bulk torque density.

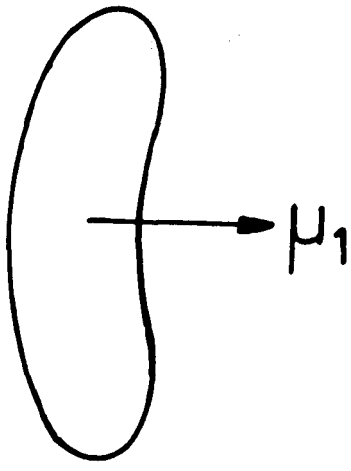

Fig.4.1: Figure showing transverse dipole moment $\mu_\perp$ of a banana shaped molecule.

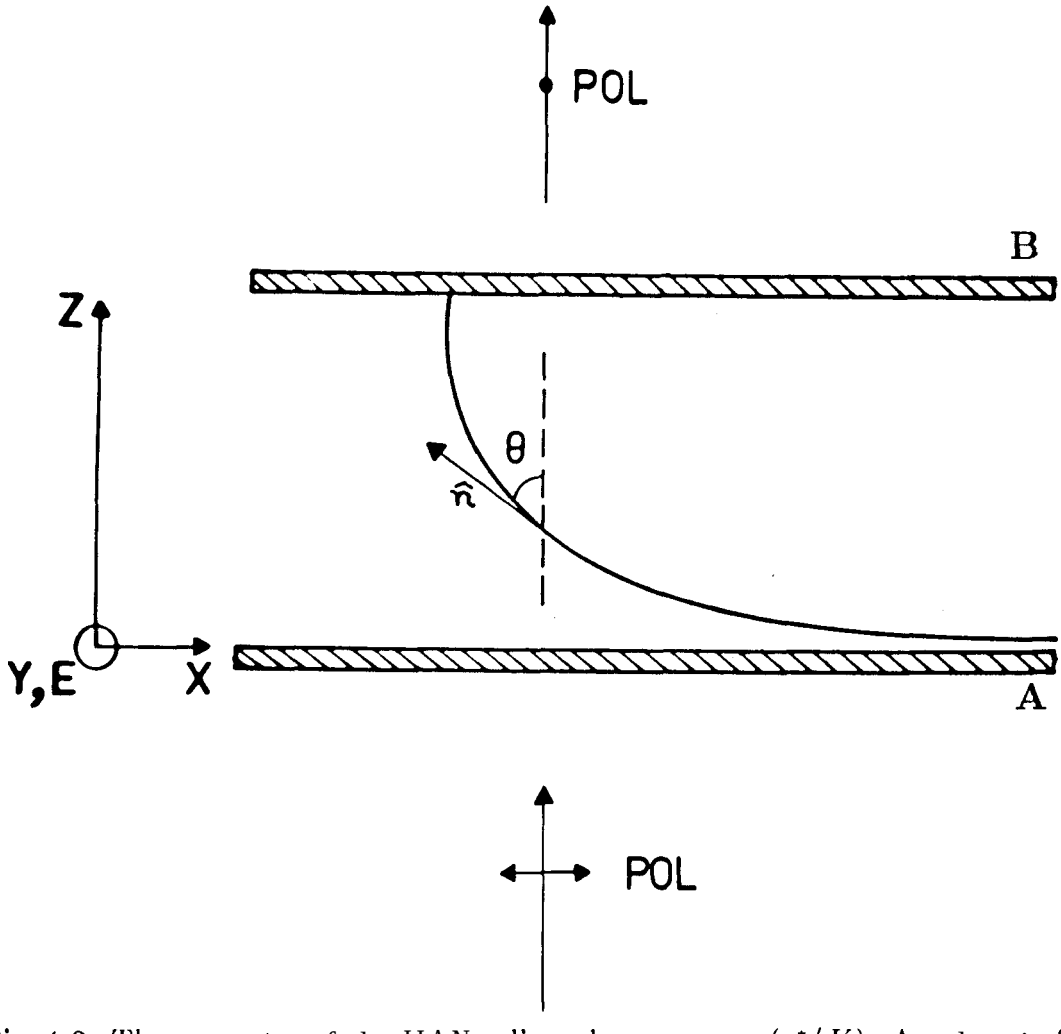

Fig.4.2: The geometry of the HAN cell used to measure (e^*/K). An electric field E_y applied perpendicular to the plane of the paper produces a twist distortion.

For small ϕ, the total energy density of the system can be written as

$$F = F^{el} + F^{flexo} + F^{\epsilon} \tag{4.3}$$

where

(a) F^{el} = the elastic free energy density

$$= \frac{K}{2}\left[\left(\frac{\partial\theta}{\partial z}\right)^2 + \sin^2\theta\left(\frac{\partial\phi}{\partial z}\right)^2\right]$$

K is the elastic constant (using the one constant approximation).

(b) F^{flexo} = flexoelectric free energy density

$$\begin{aligned} F^{flexo} &= -(P.E) \\ &= -E\left[\phi(e_3\cos^2\theta - e_1\sin^2\theta)\frac{\partial\theta}{\partial z} + e_3\sin\theta\cos 0\frac{\partial\phi}{\partial z}\right] . \end{aligned}$$

(c) F^{ϵ} = the dielectric free energy density

$$= -\frac{1}{8\pi}(\Delta\epsilon)(E\sin 0\cdot\phi)^2 .$$

Since E is a small field higher powers of E can be ignored in the linear region. The Euler-Lagrange equation (de Gcnnes, 1975) for θ

$$\frac{\partial F}{\partial\theta} - \frac{\partial}{\partial z}\left[\frac{\partial F}{\partial(\frac{\partial\theta}{\partial z})}\right] = 0 \tag{4.4}$$

and a similar one with reference to ϕ are used to minimise the energy (Eqn.4.3). The resulting equations are:

$$K\frac{d^2\theta}{dz^2} - \sin\theta\cos\theta\left(\frac{d\phi}{dz}\right)^2 + (e_1 - e_3)E\sin^2\theta\cos\phi\frac{d\phi}{dz} = 0 \tag{4.5}$$

and

$$dz\left(K\sin^2\theta\frac{d\phi}{dz}\right) - (e_1 - e_3)E\cos\phi\sin^2\theta\frac{d\theta}{dz} = 0 . \tag{4.6}$$

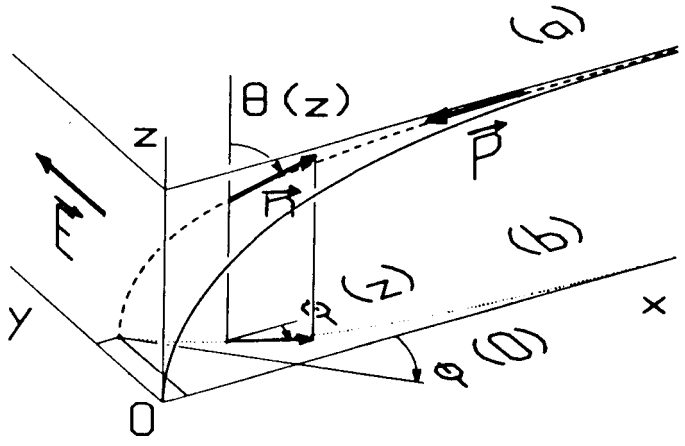

Fig.4.3: The unperturbed director pattern (in the XZ plane) twists along Y, under the action of the electric field E. The maximum twist $\phi(O)$ is observed at the homeotropic plate (after Dozov *et* al., 1982).

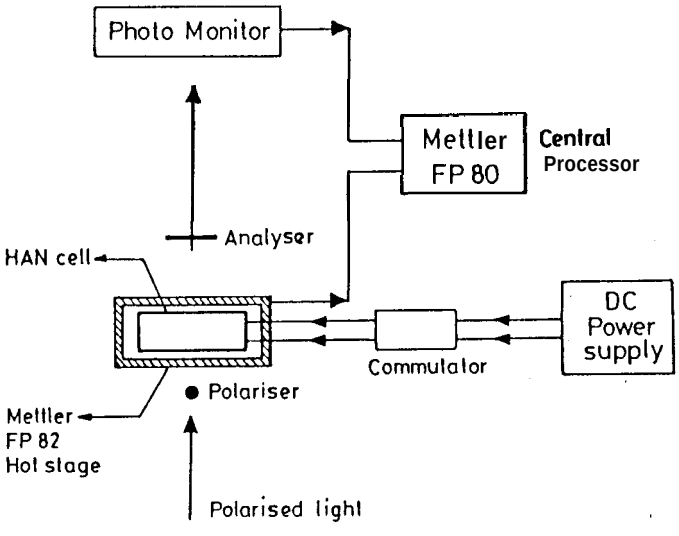

Fig.4.4: Block diagram of the experimental set up for measuring e^*/K of a NLC.

The azimutlial equation (4.6) for small fields E will give a small twist ϕ linear in E. The bend equation (4.5) describes the'change in the initial spaly-bend distortion due to the field. As we have assumed that ϕ and E are small, this change which is second order in these quantities can be neglected. Then from Eqn.(4.5) we get,

$$\frac{d^2\theta}{dz^2} = 0 \quad \text{or} \quad \theta = \frac{\pi z}{2d}$$

where d is the sample thickness.

Now linearising Eqn.(4.6) in ϕ and using $0 = \pi z/2d$, we get,

$$\frac{d\phi}{d\theta} = \left[(e_1 - e_3)\frac{Ed}{\pi K}\right] \left(\theta - \frac{1}{2} \sin 2\theta\right) \sin^{-2} \theta \ . \tag{4.7}$$

The maximum value of ϕ, i.e., $\phi(o)$ occurs close to the plate with homeotropic alignment. Equation (4.7) can be integrated exactly to get (Dozov et al., 1982)

$$\phi(o) = -\frac{(e_1 - e_3)}{K} \frac{Ed}{\pi} = -\frac{e^*}{K} \frac{Ed}{\pi} \ . \tag{4.8}$$

The block diagram of the experimental set up is shown in figure 4.4. $\phi(o)$ is measured by passing a polarised beam through the sample such that it enters the cell through the homogeneously aligned plate with the plane of polarisation parallel to the director. Since the optical phase difference is greater than the angle of twist produced in the sample, the state of polarisation follows the twisted director pattern.

It may be pointed out here that in the absence of the applied electric field, two types of domains, with opposite curvature can occur with equal probability in the sample (Fig.4.5). The flexoelectric polarisation $\vec{P}$ being in opposite directions in these domains, they twist in opposite directions when the field is applied. A mon-odomain sample is obtained by cooling the specimen from tlie isotropic pliasc in a magnetic field (of $\sim$ 5 KGauss) acting in an oblique direction which favours one of the domains over the other due to the anisotropy of tlie diamagnetic susceptibility

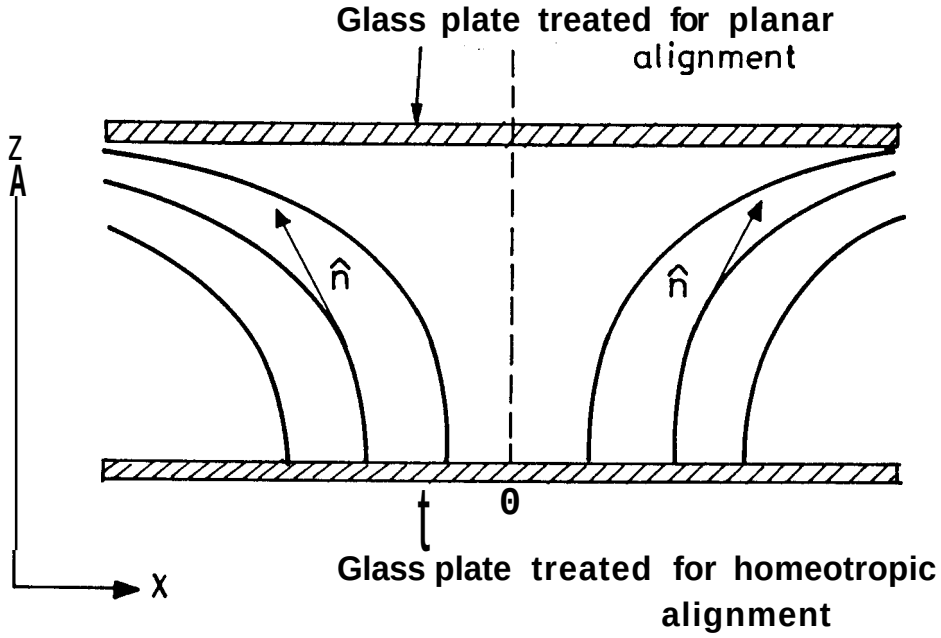

Fig.4.5: Two types of domains observed in a HAN cell in the absence of an external field.

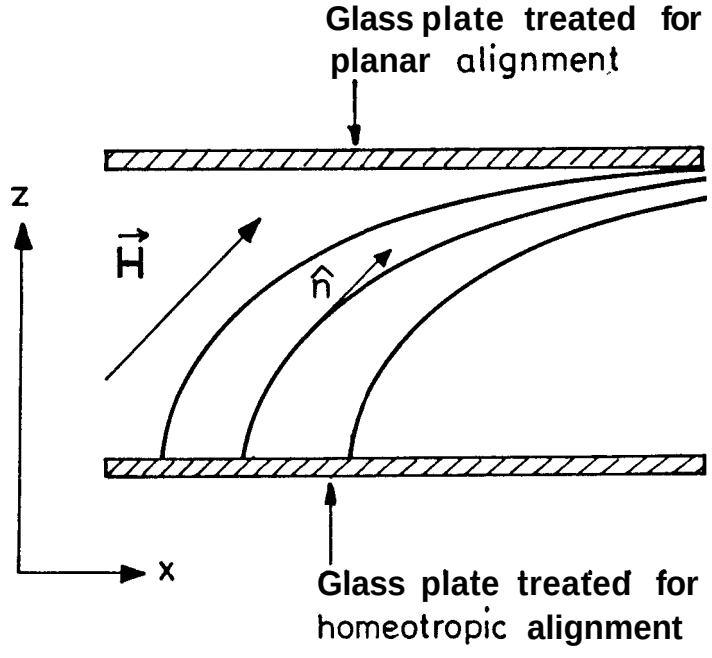

Fig.4.6: Monodomains observed in a HAN cell in the direction of the external magnetic field H.

of the material (Fig.4.6) The transverse DC electric field is applied to the HAN cell by using stainless steel wires, which also serve as spacers. The diameter of the wires used was between 35 to 50 μm. The cell is placed between crossed polarisers of a Leitz (Orthoplan) polarising microscope. A Mettler hot stage (Model FP82) is used to regulate the temperature of the sample. The HAN cell is placed such that a linearly polarised light beam with its plane of polarisation parallel to the nematic director enters the cell through the plate treated for homogeneous alignment. The transmitted light beam emerges from the plate treated for homeotropic alignment. $\phi(o)$ is measured by rotating the analyser to get the minimum intensity. In order to locate the position of minimum intensity accurately we used a Mettler photomonitor (Model ME-17517). At lower fields, the twist angle $\phi(o)$ being small ($\sim 0.5^o$), a relatively large error is associated with the $\phi(o)$ measurements. However at higher fields, the twist angle $\phi(o)$ being of the order of 2^o to 3^o the relative error is considerably reduced. We estimate that the error, which is mainly due to the measurement of $\phi(o)$ is of the order of ten per cent. e^*/K is obtained from the slope of the plot of $\phi(o)$ vs. E (Fig.4.7), and the sign of e^* is deduced from the sign of $\phi(o)$ for a given sign of E.

Figure 4.8 shows a typical experimental curve, for the highly polar compound 8CB. At higher fields, the curve is non-linear due to dielectric coupling. We use the slope of the curve in the linear region in our calculations of flexoelectric coefficients.

We have measured e^*/K for two homologous series, namely, cyanobiplienyls (nCB) and cyanoplienyl cycloliexanes (PCHn) and also for some compounds which are structurally related. Further we have also studied temperature dependences of e^*/K for most of the compounds.

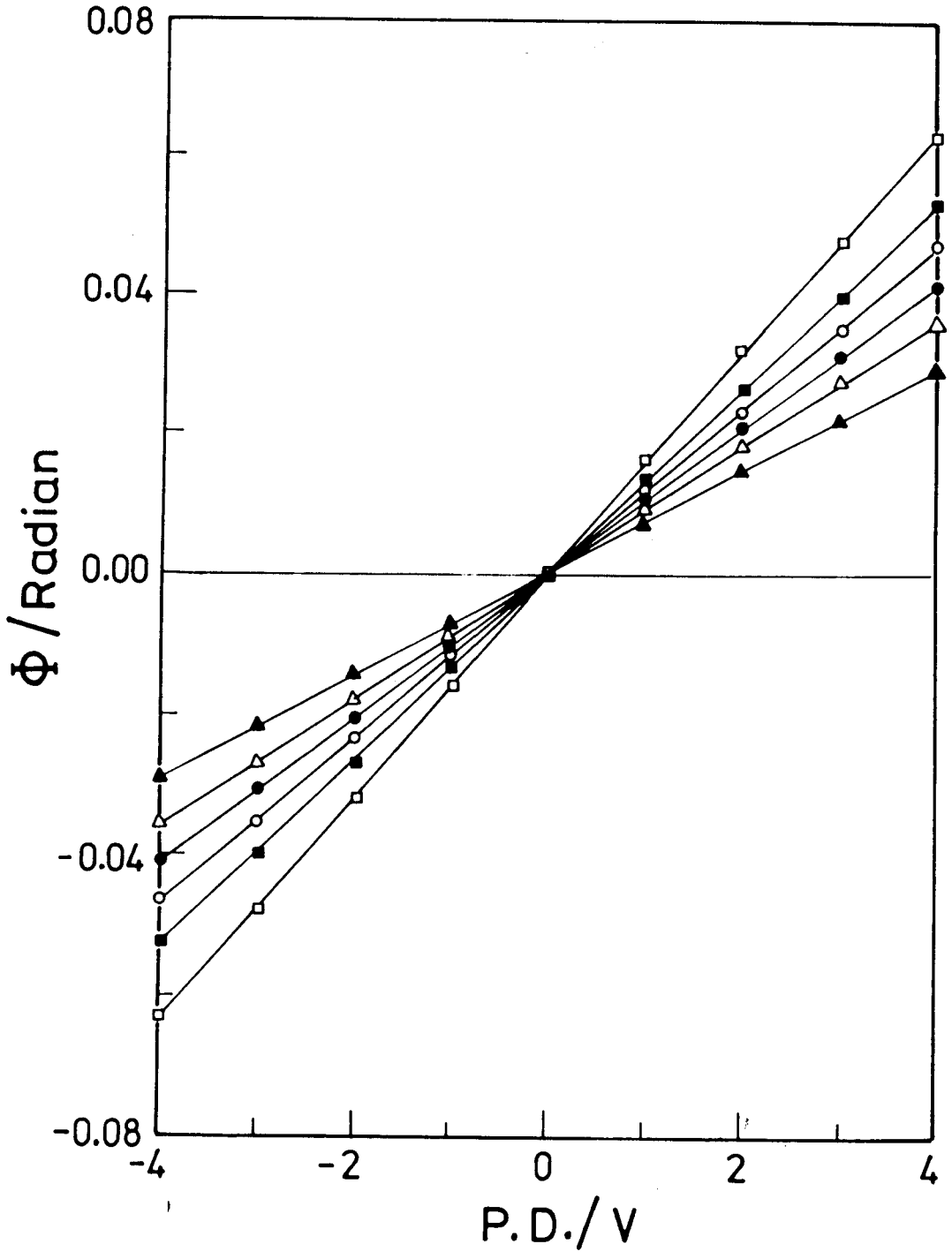

Fig.4.7: Variation of the angle of rotation (ϕ) of the plane of polarisation with applied voltage in CCH-7 at different temperatures; (A) **323** I<, **(A) 328** K, (•) **333** K, **(O)338** K, **(1)343** K and (□) **348** K.

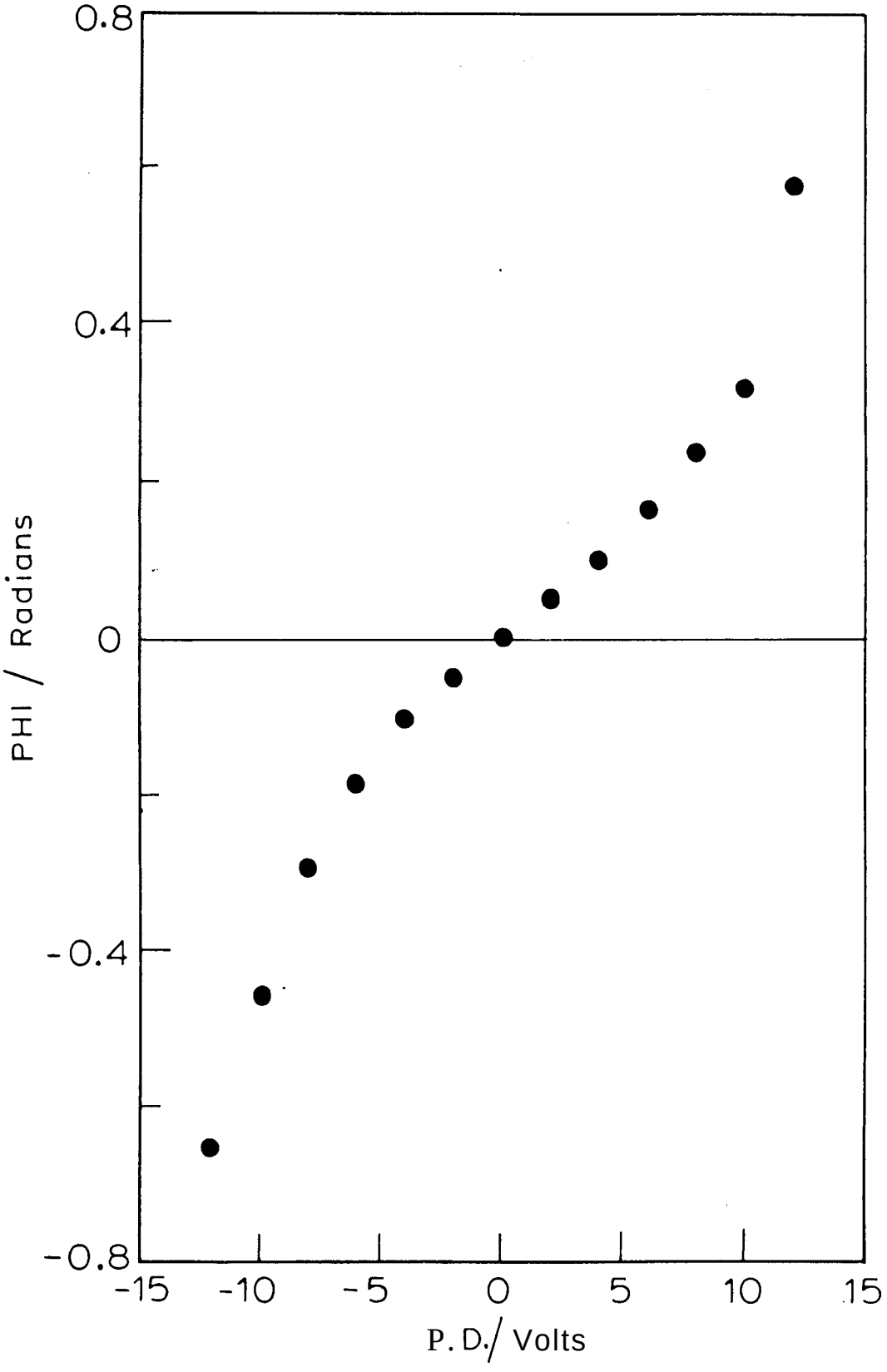

Fig.4.8: Variation of ϕ with applied DC voltage in 8CB. The linear region is between -5 V to +5 V. Beyond this region the variation of ϕ is non-linear.

4.2.2 Measurement of $(e_1 + e3)$

We have employed the technique of Dozov et al. (1984) for measuring the sum of flexoelectric coefficients $(e_1 + e_3)$. A quadrupolar field is produced by a suitable arrangement of electrodes as shown in figure 4.9. Aluminium electrodes are vacuum coated with a gap (L) of $\sim$ 1mm on an ITO plate with high resistivity. A cell of thickness $(D) \sim 50\mu m$ is constructed using two such plates, each treated with ODSE for homeotropic alignment of the nematic director with strong anchoring at the surfaces. The field gradient (Fig.4.10) set up in the cell produces a bend distortion described by the angle θ. DC voltages of $+V$ and $-$V are applied on the terminals 1,3 and 2,4 respectively to get a field gradient in the centre of the sample.

The distortion created by the field gradient is calculated in two dimensions (X,Y). In the centre of a thin cell (with L $\gg D$), by symmetry, tlie field is given by

$$\vec{E}(x,z) = -\frac{4V}{LD}(z,x) \ . \tag{4.9}$$

This matches well with the boundary conditions on the conducting plates;

$$\vec{E}(x,\pm\frac{D}{2}) = \frac{2V}{L} \quad (|x| < \frac{L}{2}) \ .$$

The field gradient produces distortion of the director which is given by the tilt angle $\theta(x,z)$. The free energy density of the nematic can be written as

$$F = F^{flex\delta} + F^{el} + F^{\epsilon} \tag{4.10}$$

where

1. The flexoelectric free energy density

   $F^{flexo} = -\vec{E} \ . \ \vec{P}$, where P is given by Eqn.(4.1).

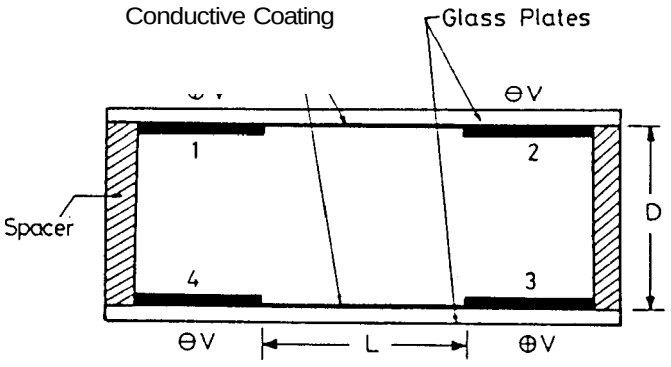

Fig.4.9: Electrode configuration used to produce a quadrupolar field. 1,2,3 and 4 are coated aluminium electrodes. The central part of *conductive coating* consists of ITO witli a high resistance. Voltages with signs as shown produce the required field distribution in the centre of the sample.

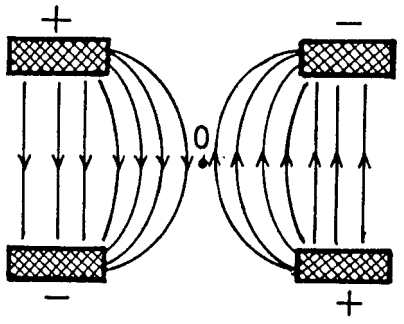

Fig.4.10: Schematic diagram showing formation of field gradient in a quadrupolar cell.

2. The elastic free energy density

$$F^{el} = \frac{1}{2}K_1(\boldsymbol{V}.\hat{n})^2 + \frac{1}{2}K_3(\hat{n} \times V \times \hat{n})^2$$

where K_1 and K_3 are the splay and bend elastic coristants respectively, and

3. The dielectric free energy density

$$F^{\epsilon} = -\frac{1}{8\pi}(\Delta\epsilon)E^2 \ .$$

For a small field close to the centre (O) of the cell, this quadratic coupling is neglected.

By minirnising the free energy density (Eqn.4.10) with respect to 6 by using the Euler-Lagrange equation (4.4), we find the equilibrium equation

$$K_1\frac{\partial^2\theta}{\partial x^2} + K_3\frac{\partial^2\theta}{\partial z^2} = \left(-\frac{4V}{LD}\right)(e_1 + e_3) \tag{4.11}$$

Since the cell is thin, we can neglect the X de endence of θ at the centre of the cell. Considering only its Z dependence, we get

$$\theta = \theta_o\left[1 - \left\{\frac{z}{(\frac{D}{2})}\right\}^2\right] \tag{4.12}$$

with

$$\theta_o = \frac{VD}{2L}\left(\frac{e_1 + e_3}{K_3}\right) \tag{4.13}$$

Note that θ is zero on the plates due to strong anchoring. Optically for small θ, the nematic cell behaves as a cell of uniform tilt, and the conoscopic pattern can be expected to rotate by an angle $n_o\bar{\theta}$, where n_o is the ordinary index of refraction and $\bar{\theta}$ is the average tilt angle in the sample given by

$$\bar{\theta} = \frac{1}{D}\int_{-D/2}^{D/2}\theta(z)dz = \frac{2}{3}\ \theta_o \tag{4.14}$$

In the absence of the field gradient, a conoscopic pattern in the form of a uniaxial cross is observed between crossed polarisers of a Leitz polarising microscope, using a monochromatic radiation from a sodium vapour lamp. The pattern will be tilted by an angle $n_o\bar{\theta}$, on applying the field gradient (Fig.4.11).

From the observed shift of the conoscopic pattern the tilt angle $\bar{\theta}$ is calculated using Mallards rule (Crossland, 1976),

$$\bar{\theta} = \sin^{-1}\left(\frac{d}{R}\right)\sin\,\theta_c\ .$$

Here $\sin\,\theta_c$ is the numerical aperture of the objective (N.A.=0.4), d is the number of divisions in the eyepiece through which the centre of the conoscopic pattern is shifted, and 2R is the number of divisions in eyepiece, covering the entire conoscopic image (see Fig.4.11).

For small angles, the above equation reduces to

$$\bar{\theta} = \frac{d}{R}\sin\theta_c = \frac{\mathrm{d}}{R} \times N.A. \qquad (4.15)$$

Using equations (4.13) and (4.15) the ratio $\left(\frac{e_1 + e_3}{K_3}\right)$ is calculated. The sign of $(e_1 + e_3)$ is deduced from the sign of θ_o for a given sign of the field gradient. The temperature of the sample is regulated by using a Mettler hot stage (1'1'82). Figure 4.12 shows the videoprints of the shift produced in the conoscopic pattern under a DC electric field in one sample.

These measurements of $(e_1 + e_3)$ have relatively large errors for the following reasons. At low fields, the field is screened due to double layer formation (Blinov, 1983). We cannot however use large fields as this will result in charge injection (at voltages above the redox potential of the liquid crystal) (Kohlmuller el *al.*, 1982) which can give rise to undesirable field gradients. Thus we applied a relatively small

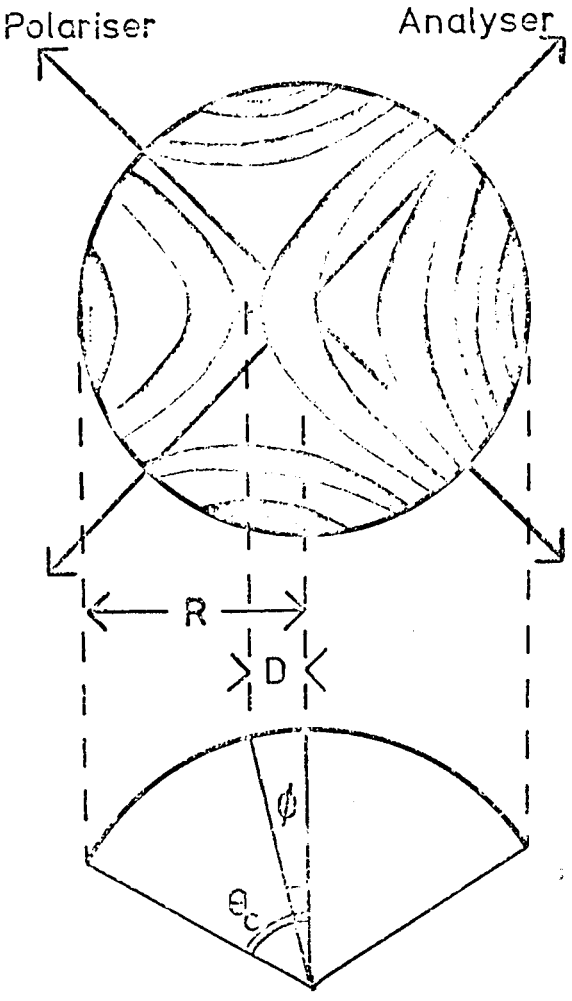

Fig.4.11: Schematic diagram showing the displacement of conoscopic pattern under the action of an electric field gradient.

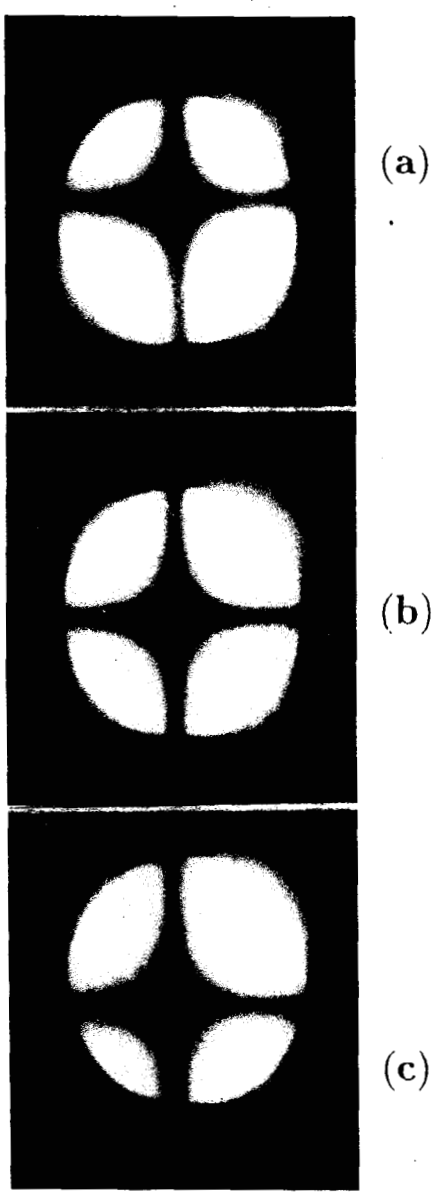

Fig. 4.12: Conoscopic pattern observed in CCH-7 at **333** K under DC electric field with polariser and analyser crossed at (a) +3 V, (b) 0 V and (c) -3 V.

voltage and the errors involved in the measurement could be $\approx$ 40%. Because of this large uncertainty, we did not measure the temperature dependence of $(\frac{e_1 + e_3}{K_3})$.

We have measured the flexoelectric coefficients $(e_1 - e_3)$ and $(e_1 + e_3)$ for a number of compounds, viz., PCHn, nCB, ROCP, 8OCB, CCH-7 and a mixture of MBB, PEC and 5CB. The structural formulae of the compounds are given in figures **4.13** and their transition temperatures in Table 4.1. These are commercial compounds obtained from Hoffmann La Roche and Merck Companies.

4.2.3 Measurement of $(e_1 + e_3)$ by using wedge shaped cell

We have also used a simpler method to measure $(e_1 + e_3)$ of NLCs having a negligible dielectric anisotropy (At-). Two indium tin oxide coated plates are treated with ODSE to get homeotropic alignment of NLC with strong anchoring at the plates. **A** wedge shaped cell is prepared as shown in the figure **4.14** using these two glass plates. On applying a DC electric field between the plates, a relatively small field gradient is developed in the cell. Since Ae of the NLC used is small, the dielectric coupling with the applied field is negligible. Neglecting **Ac,** the distortion of the director field can be calculated by equating the flexoelectric and elastic torques. Since tlic wedge angle is small, the initial bend distortion of the director field is also small. We write the director field $\hat{n} = (8, 0, 1)$ by assuming that the distortion of the director, due to an electric field E applied between the two plates is also small. The resulting components of flexoelectric polarisation along X and Z axes are

$$P_x = (\mathrm{el} + e_3)\,\theta\,\frac{\partial 0}{\partial x} + e_3\,\frac{\partial 0}{\partial z} \tag{4.16}$$

$$P_z = -(e_1 + e_3)\,\theta\,\frac{\partial \theta}{\partial z} + e_1\,\frac{\partial \theta}{\partial x}\ . \tag{4.17}$$

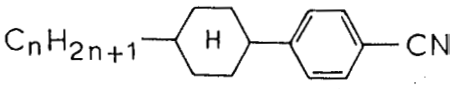

n = 3,4,5,7

Trans – 4-n-Alkyl-(4 - cyanophenyl) - cyclohexane

[PCH - series]

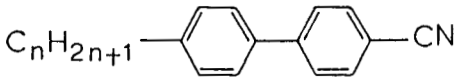

n = 5-8

4'-n-Alkyl-4-cyanobiphenyl

[CB - series]

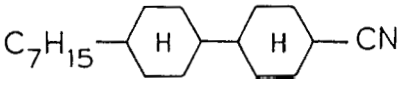

n – Heptyl cyano cyclohexylcyclohexane

[CCH-7]

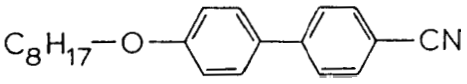

4'-n-Octyloxy-4- cyanobiphenyl

[8 OCB]

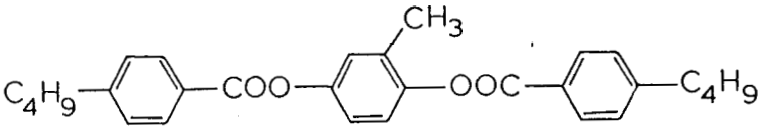

2-Methylphenyl - bis-4-n- butylbenzoate

[RO-CE 1700]

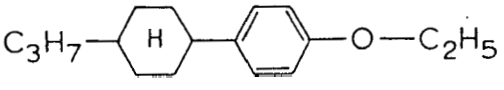

1-n-propyl-4(4-n-ethoxyphenyl) cyclohexane

[PCH-302]

Fig.4.13: The structural formulae of the compounds studied.

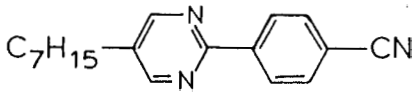

5-n-Heptyl-2-(4-cyanophenyl)-Pyrimidine

[HCP]

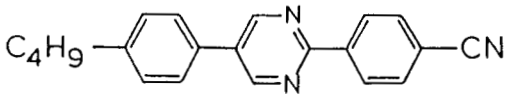

5-(4-n-Butylphenyl)-2-4-cyanophenyl)-Pyrimidine

[BPCP]

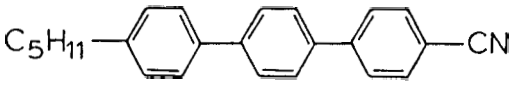

4''-n-Pentyl-4-Cyano-p-terphenyl

[5-CT]

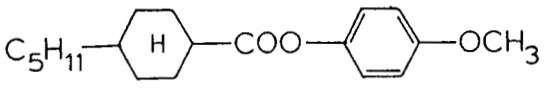

4-Methoxyphenyl-trans-4-n-Pentylcyclohexylcarboxylate

[M.P.P.C]

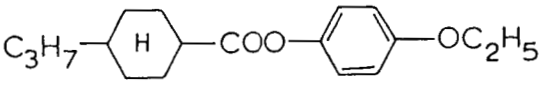

4-Ethoxyphenyl-trans-4-n-Propylcycloxylcarboxylate

[E.P.P.C]

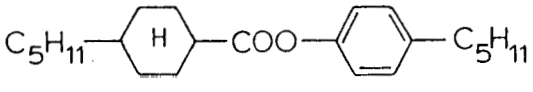

4-Pentylphenyl-trans-4-n-Pentylcyclohexylcarboxylate

[P.P.P.C]

Fig.4.13(contd.): The structural formulae of the compounds studied.

Table 4.1: LIST OF COMPOUNDS STUDIED

Symbol	Chemical narne	Clearing point (in K)	$(e_1 - e_3)/K_2$ $\times 10^{-2}$ CN^{-1}m^{-1} (at Temp.)	$(e_1 + e_3)/K_3$ $\times 10^{-2}$ CN^{-1}m^{-1} (at Temp.)
PCH-3	trans-4-Propyl-(4-cyanophenyl). cyclohexane	317.5	36(310 K)	11(310 K)
PCH-4	*trans*-4-Butyl-(4-cyanophenyl)-cyclohexane	312	155(311 K)	
PCH-5	*trans*-4-Pentyl-(4-cyanophenyl)-cyclohexane	324.2	166(303 K)	12(303 K)
PCH-7	*trans*-4-Heptyl-(4-cyanophenyl)-cyclohexane	327	120(303 K)	23(303 K)
5CB	4′-n-Pentyl-4-cyanobiphenyl	307.8	240(303 K)	108(303 K)
6CB	4′-n-Hexyl-4-cyanobiphenyl	302	251(301 K)	
7CB	4′-n-Heptyl-4-cyanobiphenyl	312.6	353(303 K)	
8CB	4′-n-Octyl-4-cyanobiphenyl	312	228(307 K)	
CCH-7	Heptylcyanocyclohexylcyclohexane	355.7	-129(343 K)	51(343 K)
ROCP-7037	5-n-Heptyl-2-(4-cyanophenyl)-pyrimidine	323.5	436(319 K)	5(319 K)
ROCP-7334	5-(4-n-Butylphenyl)-2-(4-cyano-phenyl)-pyrimidine	517.7	252(373 K)	16(373 K)
5CT	4′-n-Pentyl-4-cyano-p-terphenyl	511.5	87(423 K)	
MPPC	4-Methoxyphenyl-*trans*-4-pentyl-cyclohexylcarboxylate	344	52(323 K)	
EPPC	4-Ethoxyphenyl-*trans*-4-propyl-cyclohexylcarboxylate	351	28(323 K)	
PPPC	4-Pentylphenyl-*trans*-4-pentyl-cyclohexylcarboxylate	320	297(310 K)	
8OCB	4′-n-Octyloxy-4-cyanobiphenyl	352.6		29(343 K)
Mixture of MBB (46%) PEC (50%) and 5CB (4%)	1,4-di-(4-butylbenzoyloxy)-2-methylbenzene 1-n-Propyl-4(4-n-ethoxyphenyl)-cyclohexane 4′-n-Pentyl-4-cyanophenyl	342	33(303 K)	-60(303 K)

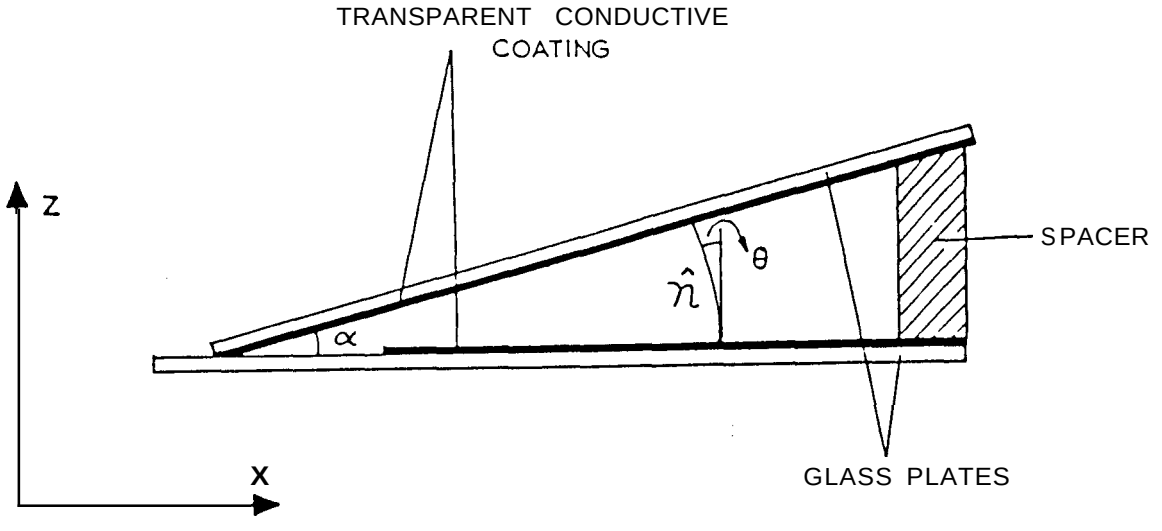

Fig.4.14: Schematic diagram of the wedge shaped cell used in the measurement of $(e_1 + e_3)$ of materials with low values of dielectric anisotropy ((Ar).

Minimising the flexoelectric free energy density $f^{fl} = -P \cdot E$ and neglecting higher order terms, the flexoelectric torque becomes,

$$\Gamma^{fl} = e_3 \frac{\partial E_x}{\partial z} + e_1 \frac{\partial E_z}{\partial x} \quad . \tag{4.18}$$

From Maxwell's equation, V x $E = 0$ we get,

$$\frac{\partial E_x}{\partial z} = \frac{\partial E_z}{\partial x} \quad . \tag{4.19}$$

Using Eqn.(4.19) in Eqn.(4.18), we get flexoelectric torque,

$$\Gamma^{fl} = (e_1 + e_3) \frac{\partial E_z}{\partial x} \quad . \tag{4.20}$$

In the one elastic constant approximation, the elastic free energy density is given by

$$F^d = \frac{1}{2} K \left(\frac{\partial \theta}{\partial z} \right)^2 \quad . \tag{4.21}$$

Minimising this elastic free energy density, the elastic torque is written as

$$\Gamma^d = -K \frac{\partial^2 \theta}{\partial z^2} \quad . \tag{4.22}$$

Equating the flexoelectric torque with elastic torque given by equations (4.21) and (4.22) we get

$$(e_1 + e_3) \frac{\partial E_z}{\partial x} = K \frac{\partial^2 \theta}{\partial z^2} \quad . \tag{4.23}$$

The boundary conditions to be satisfied by the director are

$$\theta(z = 0) = 0 \quad \text{and} \quad \theta(z = \mathrm{d}) = \alpha$$

where α is the wedge angle. The solution of eqn.(4.23) satisfying the above boundary conditions is obtained as

$$\theta(z) = \left[\frac{(e_1 + e_3) V \alpha}{2K} \right] \left[\frac{z}{d} - \left(\frac{z}{d} \right)^2 \right] + \frac{\alpha z}{d} \quad . \tag{4.24}$$

where V is the applied voltage.

As in the previous method (4.2.2), θ is obtained from the tilt of the conoscopic pattern observed between crossed polarisers. For small θ the conoscopic pattern can be expected to rotate by an angle $n_o\bar{\theta}$, where n_o is the ordinary refractive index and 0 is the average tilt angle in the sample given by

$$\bar{\theta} = \frac{1}{d}\int_o^d \theta(z)dz$$

$$= \left(\frac{\alpha}{2}\right)\left[1 + \frac{(e_1 + e_3)V}{6K}\right] \tag{4.25}$$

The first term on the right hand side of this equation gives the tilt of the conoscopic pattern due to the initial bend distortion of the director field and the second term gives the tilt due to the flexoelectric distortion. Since the latter depends on the sign of the applied field, the pattern should shift in the opposite direction when the field is reversed. By measuring the shift of the conoscopic pattern $(e_1 + e_3)$ is estimated. The sign of $(e_1 + e_3)$ is obtained from the direction of the tilt of the conoscopic pattern for a given sign of the field.

Using this method we have measured $(e_1 + e_3)$ for a mixture of 48 mole % ROCHE-1700 and 52 mole % PCH-302 (see Fig.4.13 for the molecular structures). This mixture has $\Delta\epsilon \simeq 0$ and has been used in our studies on EHD instabilities.

4.3 Results and Discussion

We have measured the flexoelectric coefficients of the compounds listed in Table 4.1. We can note the following general trends:

1. e^*/K has a positive sign in practically all the compounds, except CCH-7 , which has a negative value.

2. e^*/K is independent of temperature in most of the compounds, i.e., $e^* \propto S^2$ as is theoretically expected (figures 4.15 and 4.16).

3. However in the case of CCH-7, MPPC, EPPC and PPPC, the absolute value of e^*/K increases with temperature (Fig.4.17.)

4. The magnitude of e^*/K increases when the cyclohexane ring is replaced by a phenyl ring. This can be clearly seen by comparing the seventh homologues of different series. e^*/K which is negative for CCH-7, becomes positive for PCH-7 and increases further in 7CB.

5. The magnitude of e^*/K decreases when we go from a two benzene ring to a three benzene ring system (for example 5CB to 5CT).

6. e^*/K is not very sensitive to chain length.

7. For all the single component systems for which $(e_1 + e_3)$ measurements have been made, the sign of $(e_1 + e_3)$ is positive. But in the mixture consisting of MBB, PEC and 5CB the sign of $(e_1 + e_3)$ is negative. This mixture also has opposite signs for $(e_1 - e_3)$ and $(e_1 + e_3)$ as in the case of CCH-7.

8. Beresnev et *al* (1987) measured e_1 of 5CB by a pyroelectric technique and obtained a value of 0.5 x $10^{-11} C/m$. Our value is comparable to this.

9. Marcerou and Prost (1980) measured $(e_1 + e_3)$ of 80CB by using interdigital electrode technique and got a value of $(2.1 \pm 0.5)10^{-11} C/m$ at 346 K. Our value is $+(0.6 \pm 0.2)$ x $10^{-11} C/m$, which is somewhat lower. But the sign and magnitude that we obtain agree with the corresporiding measurements by Dozov et al. (1984).

10. Experimentally we measure e^*/K, where the relevant value of **K'** is the twist elastic constant K_2. In many cases, K_2 is known to deviate considerably from the mean field dependence of S^2. In the case of CCH-7 we estimated the value of e* using the known values of K_2 (Schad and Osman, 1981). We have also calculated e^*/S and e^*/S^2 taking the measured value of the order

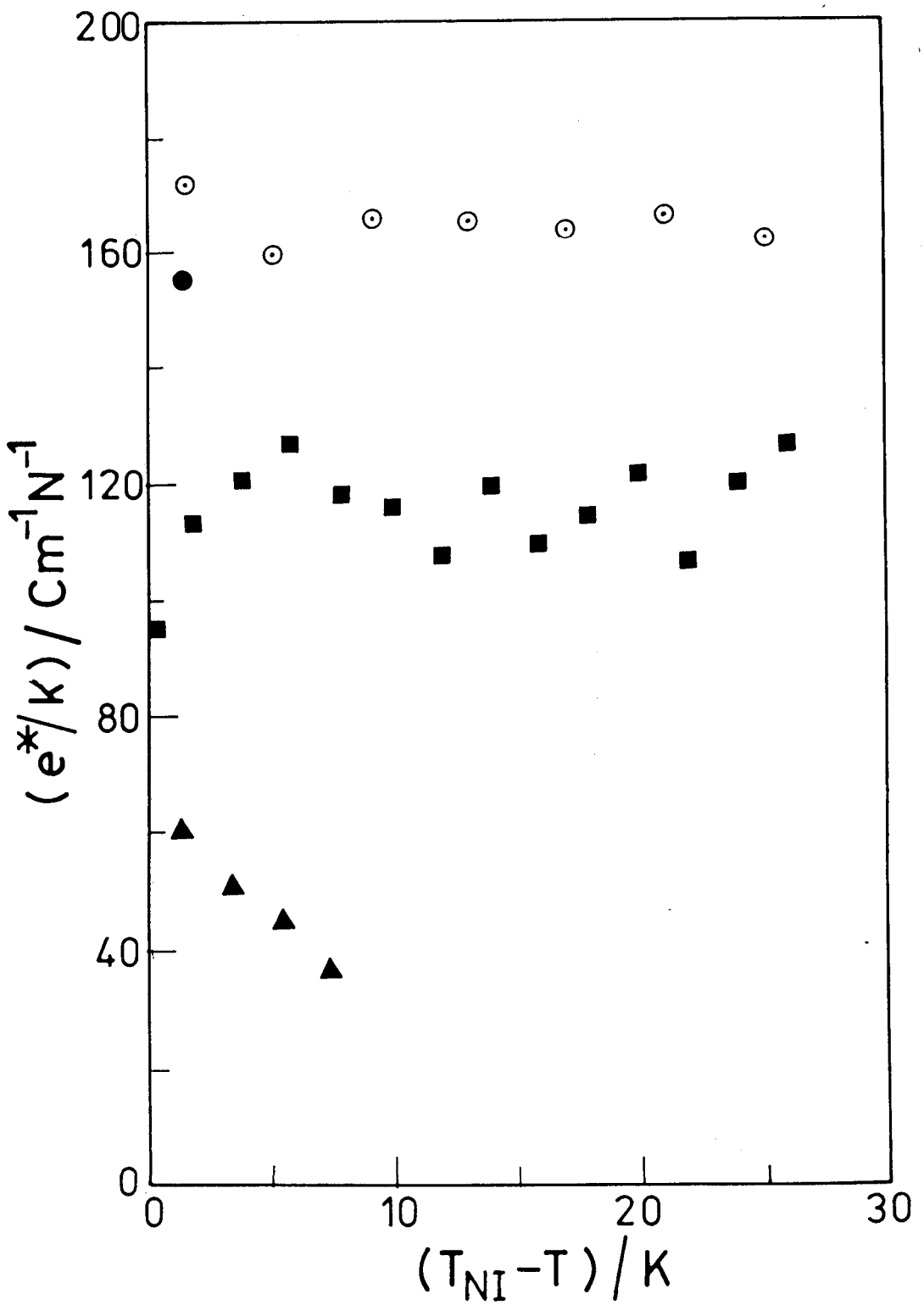

Fig.4.15: Variation of (e^*/K) with relative temperature $(T_{NI} - T)$ for the phenyl cyclohexane series (■) PCH-7, (⊙) PCH-5, (●) PCH-4, and **(A)** PCH-3. Tlie number of data points in PCII-3 are less due to a narrow temperature range of nematic phase. The variation is within the experimental error.

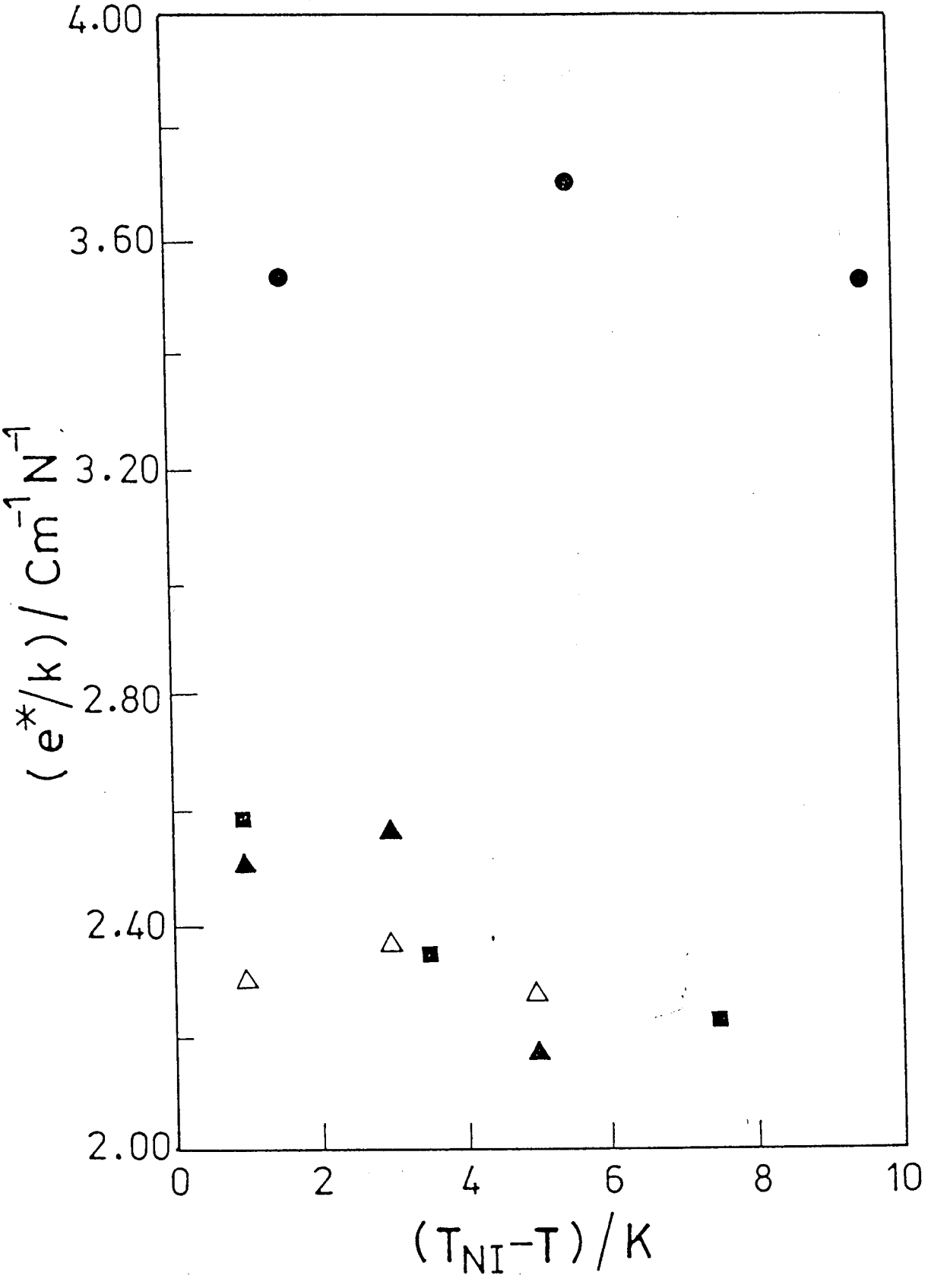

Fig.4.16: Variation of (e^*/K) with relative temperature $(T_{NI} - T)$ for cyanobiphenyl series. (A)8CB, (O)7CB, (A)6CB and (■) 5CB.

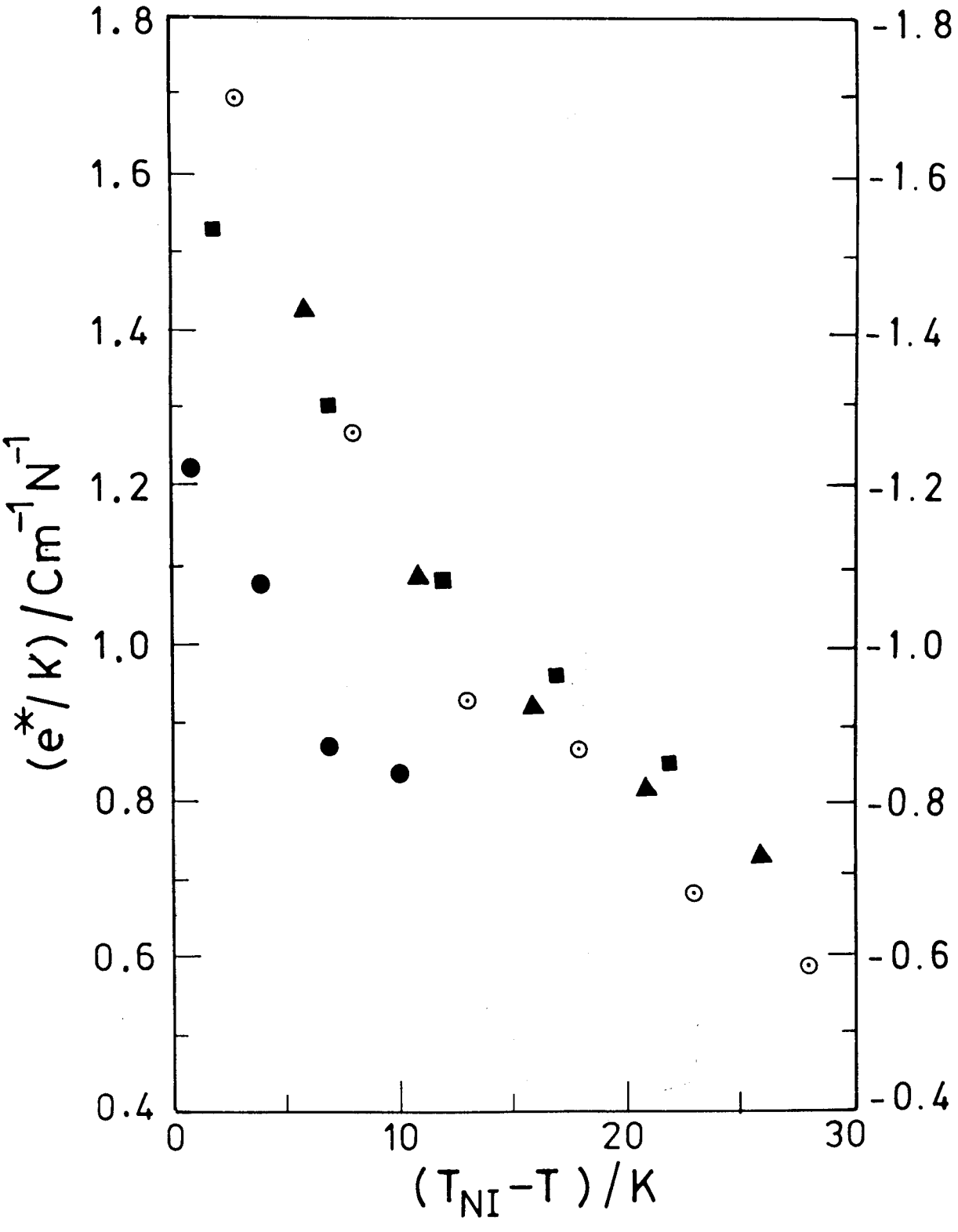

Fig.4.17: Variation of (e^*/K) with relative temperature $(T_{NI} - T)$ for (▲) MPPC, (⊙) EPPC, (●) PPPC and (■) CCII-7. Note that e^*/K is *negative* for CCII-7 (scale on right hand side.)

parameter, S (Schad et al., 1979). In order to have a better comparison of the temperature dependence of the ratios, we have normalised them with respect to their average values over the given temperature range (see Fig.4.18). From the graph it is clear that $e^* \propto S$ in the case of CCH-7. On the other hand, similar plots for PCH-7 (Fig.4.19) and 7CB (Fig.4.20) clearly show that $e^* \propto S^2$ in these cases.

As we have discussed in the introduction, the main contribution to e^* arises from permanent dipoles. As we have also noted the molecular models (Straley, 1976; Osipov, 1983,1984) lead to the result that e^* arises mainly from the transverse dipole moments of molecules with shape asymmetry. Thus it is interesting that the cyanophenyl cyclohexanes as well as cyanobiphenyls have a significant value of e^*/K though in both of them the permanent dipole is a terminal cyano group which is oriented towards the aromatic core. However we note that the aromatic core has a high polarisability. Further, both cyanobiphenyls (CB) and PCH compounds have relatively low N-I transition points. Consequently, we can assume that the alkyl chain has the all-trans conformation in these compounds (Marcelja, 1974). This would give a naturally bowed structure (Figures 4.21 and 4.22). As the dipole moment induced in the aromatic core by the end cyano group is no longer strictly parallel to the long axis of such a molecule, it produces a reasonable transverse component. In fact this gives rise to a negative sign of e_3 which in turn gives rise to a positive value of e^* in these compounds. Further, comparing homologues of PCH and CB series, the latter have lower values of the nematic-isotropic transition temperatures, and also have the more polarisable biphenyl cores. Due to both of these reasons, we get higher values of e^*/K in the cyanobiphenyls. On the other hand, in pentyl cyanoterphenyl, e^*/K actually decreases cornpared to 5CB. We must however note here that $T_{NI} = 512^oK$ in 5CT and the alkyl chain can no

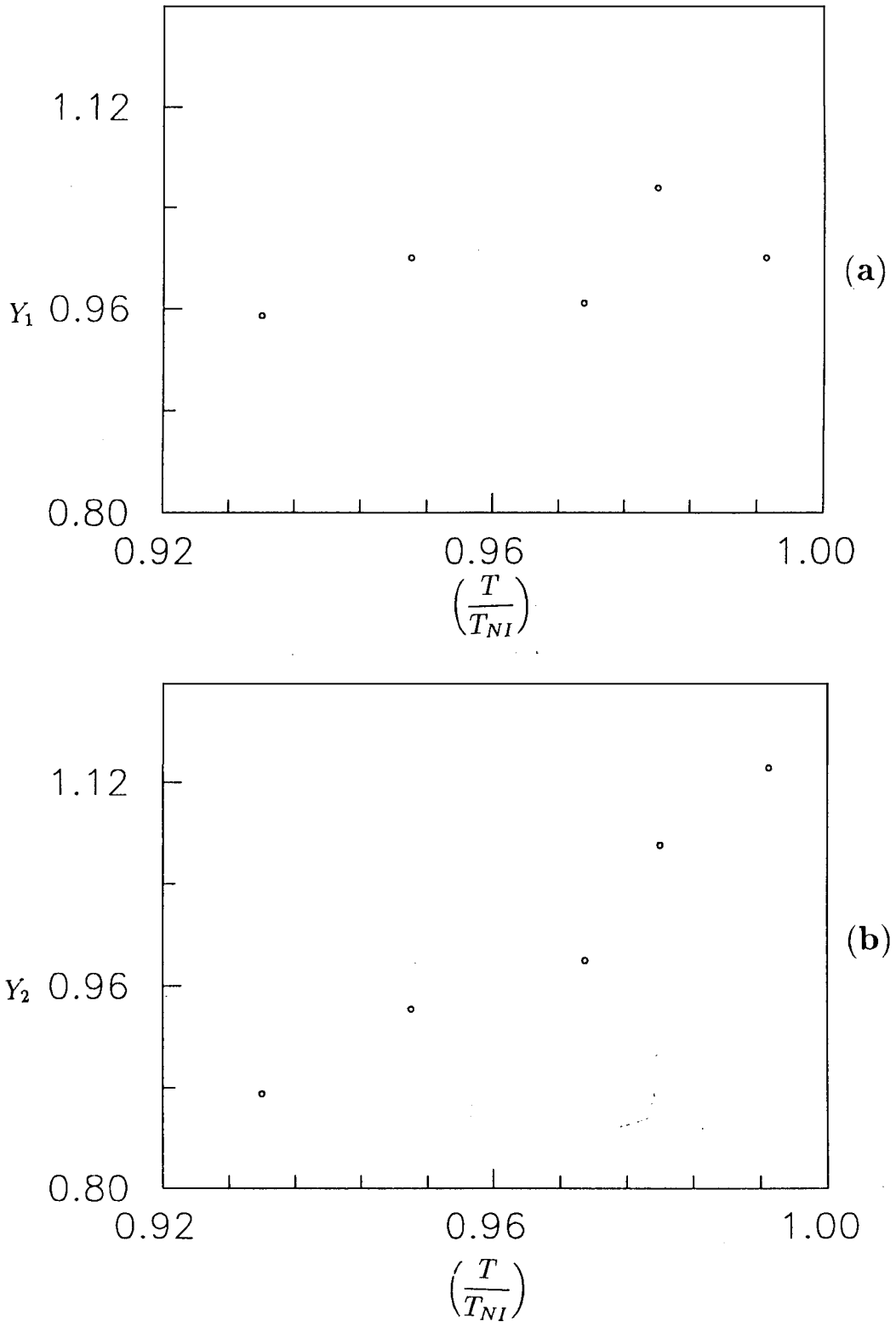

Fig.4.18: Temperature variation of (a) $Y_1 = \frac{(e^*/s)}{(e^*/s)_{Av}}$ and (b) $Y_2 = \frac{(e^*/s^2)}{(e^*/s^2)_{Av}}$ for CCH-7.

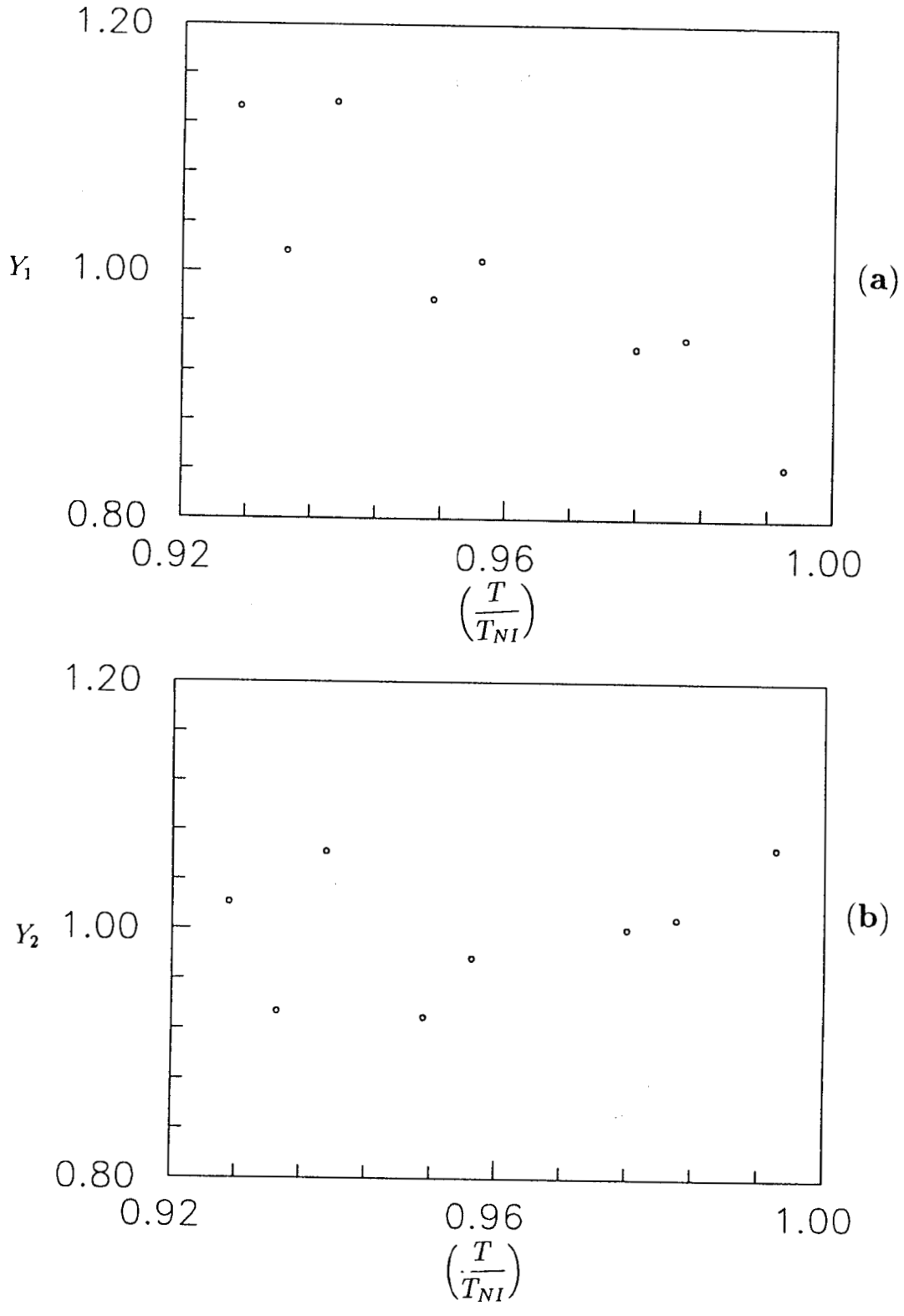

Fig.4.19: Temperature variation of (a) $Y_1 = \frac{(e^*/s)}{(e^*/s)_{Av}}$ and (b) $Y_2 = \frac{(e^*/s^2)}{(e^*/s^2)_{Av}}$ for PCH-7.

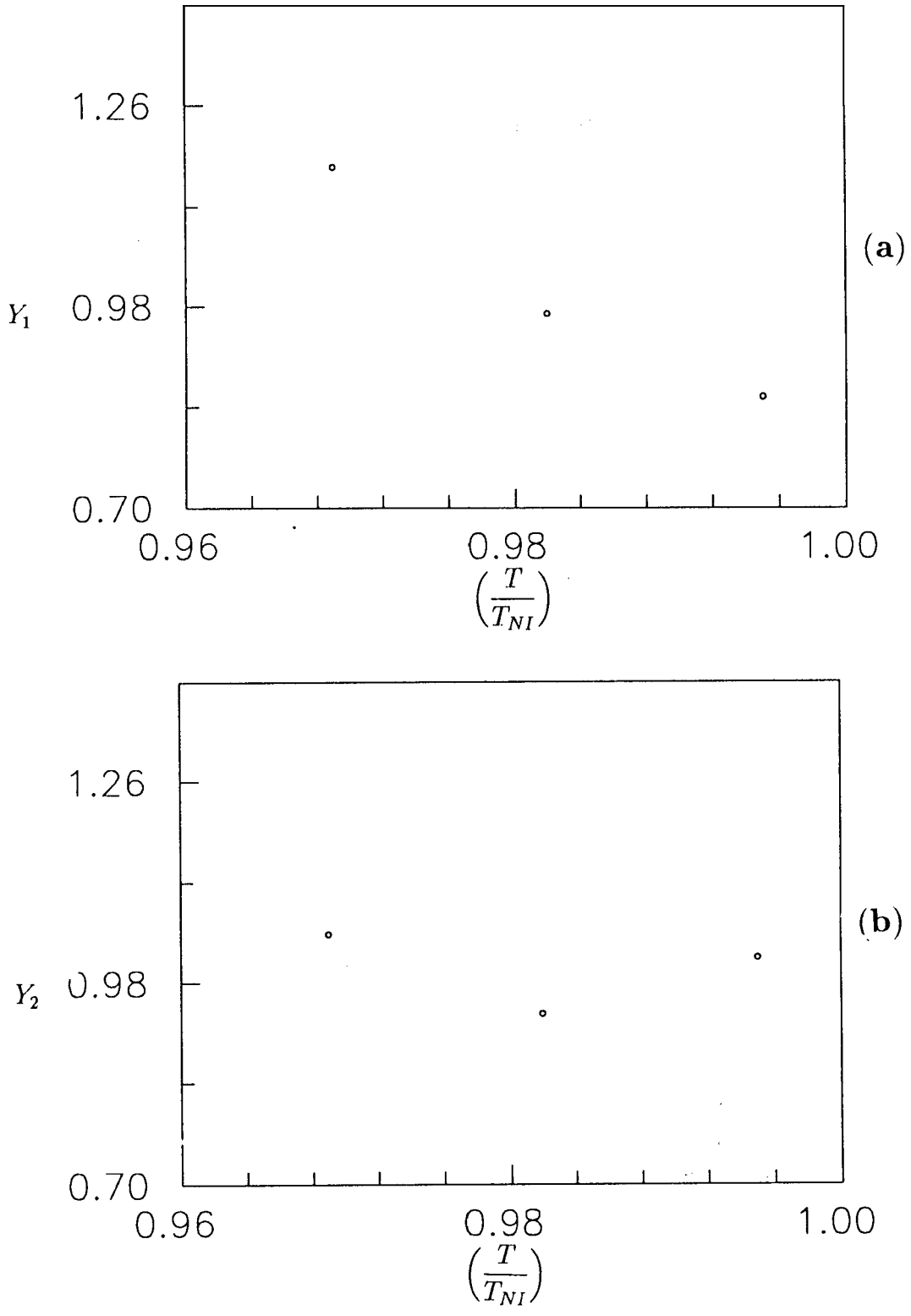

Fig.4.20: Temperature variation of (a) $Y_1 = \frac{(e^*/s)}{(e^*/s)_{Av}}$ and (b) $Y_2 = \frac{(e^*/s^2)}{(e^*/s^2)_{Av}}$ for 7CB.

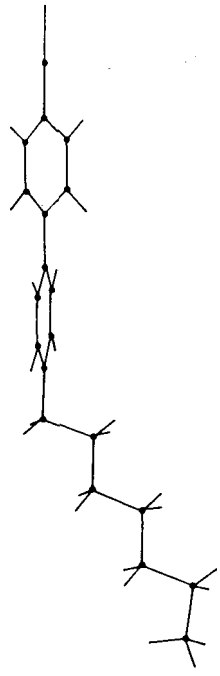

Fig.4.21: Molecular structure of 7CB. The all trans-configuration of the heptyl chain gives rise to a bent structure. The dipole moment induced in the biphenyl part by the end cyano group has a non-zero transverse component in relation to the effective long axis of the bent molecule.

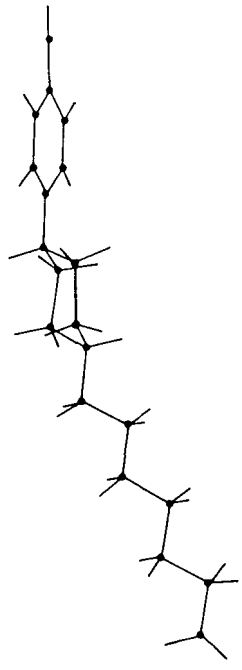

Fig.4.22: Molecular structure of PCH-7. As in Fig.4.20, note the bent structure due to the trans heptyl chain. The induced dipole in the phenyl ring would be smaller than in 7CB.

longer be considered to be in an all-trans configuration (Marcelja, 1974). Thus the shape of the molecule is no longer bowed and thus $|e_3|$ and hence $|e^*/K|$ decreases in magnitude. This trend is also seen in pyrimidine compounds: as the aromatic core size is increased, the transition temperature increases and e^*/K decreases.

In CCH-7, on the other hand, the end cyano group makes a non-negligible angle with the long axis of the molecule. Though CCH-7 can be expected to have a fairly straight configuration (Fig.4.23a) in the lowest energy state, there is considerable rotational freedom around the single C-C bond between the two cyclohexane rings. Thus bent configurations (as in Fig.4.23b) can occur in the molecule. The nematic-isotropic transition temperature in this case is high enough (355 K) to produce such configurations. Further, as the temperature is increased, the molecule adopts the bent configuration more frequently thus increasing the effective value of e_3. Further, the transverse dipole moment which is effective in the bent configuration has tlic opposite direction compared to that in PCH-7 and 7CB molecules. Thus the sign of e_3 and hence that of $(e_1 - e_3)$ reverses in CCII-7. Arguments similar to tlie above can be extended to the case of MPPC, EPPC and PPPC, in which there is a $-C\lesssim^{O}_{O}$ bridging group between a cyclohexane and a phenyl rings. In these compounds, there is a relative increase in the number of conformations producing bent structures with temperature, leading to tlie observed increase of e^*/K with temperature. In this context, we recall that Dozov et al. (1983) found a similar increasing trend of e^*/K with temperature in 8OCB. They attributed this unusual result to the entropic effects arising from the flexibility of the alkyl chains, a point which was later elaborated by Osipov (1984). However, as we have discussed in the case. of 5CT, if the flexibility is too high it cannot be expected to give rise to an additional contribution to the temperature variation of e^*.

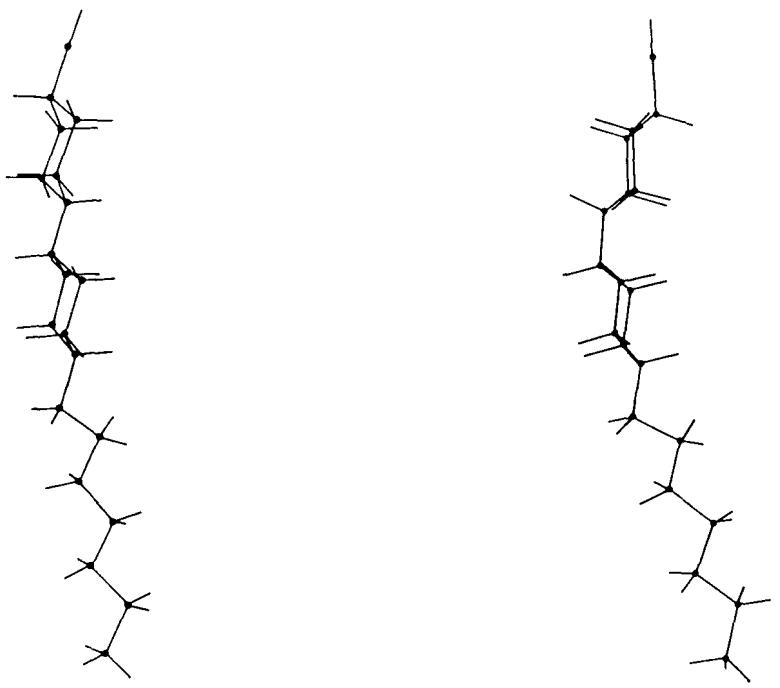

Fig.4.23(a): Molecular structure of CCH-7. Note that in the ground state the molecule is nearly straight.

(b): A rotation about the C-C bond between the two rings produces a bent structure in CCM-7. Note that the dipole of the cyano end group has an opposite transverse component in the bent upper moiety compared to PCH-7.

References

BARBERO,G., TAVERNA VALABREGA, P., BARTOLINO,R., and VALENTI,B., 1986, Liquid Crystals, 1, 483.

BERESNEV,L.A., BLINOV,L.M., DAVIDYAN,S.A., KONONOV,S.G., and YABLONSKII,S.B., 1987, JETP Lett., 45, 755.

BLINOV,L.M., 1983, *Electrooptical* and Magnetooptical Properties of Liquid Crystals, John Wiley & Sons Ltd.

CROSSLAND,W.A., MORRISSY,J.H., and NEEDHAM,B., 1976, J. Phys. D; *Appl.* Phys., **9,** 2001.

DE GENNES,P.G., 1975, The Physics of Liquid Crystals, Clarendon, Oxford.

DOZOV,I., MARTINOT-LAGARDE,Ph., and DURAND,G., 1982, J. de Phys. Lett., 43, L-365.

DOZOV,I., MARTINOT-LAGARDE,Ph., and DURAND,G., 1983, J. *de* Phys. Lett., 44, L-817.

DOZOV,I., PENCHOV,I., MARTINOT-LAGARDE, Ph., and DURAND,G., 1'384, *Ferroelectric Lett.*, 2, 135.

HELFRICH,W., 1971a, *Z.Naturforsch.*, **26a**, 833.

HELFRICH,W., 1971b, Phys. Lett., **35A**, **393.**

HELFRICH,W., 1974, Appl. Phys. Lett., 24, 451.

KOHLMULLER,H., and SIEMSEN,G., 1982, Siemens *Forsch - U.Entwickl-Ber*, Bd **11, Nr.5**, 229.

MADHUSUDANA,N.V., and DURAND,G., 1985, J. de Phys. Lett., 46, L-195

MADHUSUDANA,N.V., RAGHUNATHAN,V.A., and SUMATHY,K.R., 1987, Pramana - J. Phys., 28, L311.

MADHUSUDANA,N.V., and RAGHUNATHAN,V.A., 1989, Liquid Crystals, 5, 1789.

MARCELJA,S., 1974, J. Chem. Phys., 60, 3599.

MARCEROU,J.P., and PROST,J., 1980, Mol. *Cryst.* Liquid *Cryst.*, 58, 259.

MEYER,R.B., 1969, Phys. Rev. Lett., 22, 918.

NEMTSOV,V.N., and OSIPOV,M.A., 1986, *Sov. Phys. Crystallog.*, 31, 125.

OSIPOV,M.A., 1983, *Sov.* Phys. JETP, 58, 1167.

OSIPOV,M.A., 1984, J. de Phys. Lett., 45, L-823.

PROST,J., and MARCEROU,J.P., 1977, J. de Phys., 38, 315.

RAGHUNATHAN,V.A., MAHESWARA MURTHY,P.R., and MADI-IUSUDANA, N.V., 1991, Mol. *Cryst.* Liquid *Cryst.*, 199, 239.

SCHAD,Hp., BAUR,G., and MEIER,G., 1979, J. *Chem. Phys.*, 71, 3174.

SCHAD,Hp., and OSMAN,M.A., 1981, J. Chem. Phys., 75, 880.

SKALDIN,O.A., LACHINOV,A.N., and CHUVYROV,A.N., 1985, *Sov.* Phys. *Solid* State, **27,** 734.

SKALDIN,O.A., and CHUVYROV,A.N., 1990, *Sov.* Phys. Crystallogr., 35, 605.

SINGH,Y., and SINGH,U.P., 1989, *Phys.* Rev., A39, 4254.

STRALEY,J.P., 1976, Phys. Rev., **A14,** 1835.